

Experimental demonstration of the coexistence of spin Hall and Rashba effects in β -tantalum/ferromagnet bilayers

Gary Allen, Sasikanth Manipatruni, Dmitri E. Nikonov, Mark Doczy, and Ian A. Young

Components Research, Intel Corporation, Hillsboro, Oregon 97124, USA

(Received 3 December 2014; revised manuscript received 23 February 2015; published 16 April 2015)

We have measured the spin torques of β -tantalum/Co₂₀Fe₆₀B₂₀ bilayers versus Ta thickness at room temperature using a ferromagnetic resonance (FMR) technique. A significant fieldlike spin torque originating from Ta was identified, which is constant and independent of Ta thickness. Because of this constant torque, the spin Hall coefficient θ_{SH} needs to be calculated from the ratio of the symmetric component of the FMR signal to the slope of the antisymmetric component with Ta thickness, from which a value of -0.11 ± 0.01 was determined. The saturation magnetization of the CoFeB layers for samples deposited with Ta was found to be smaller than that of a single CoFeB layer, with values of 1.84 ± 0.01 and 1.92 ± 0.01 T, respectively. The origin of the fieldlike torque is ascribed to an interface spin-orbit coupling, or Rashba effect, due to the strength and constancy of the torque with Ta thickness. From fitting measured data to a semiclassical diffusion model that includes interface spin-orbit coupling, we have determined the spin diffusion length for β -tantalum to be 2.5 nm.

DOI: [10.1103/PhysRevB.91.144412](https://doi.org/10.1103/PhysRevB.91.144412)

PACS number(s): 72.25.Ba, 72.25.Mk, 76.50.+g, 75.70.Tj

I. INTRODUCTION

Complementary metal-oxide-semiconductor (CMOS) integrated circuits have been scaled over the past four decades and will continue for at least another 15 years [1]. At the same time, research in beyond-CMOS devices [2–4] is being actively pursued. The main driving force of this research is the need for low-power logic circuits [5] as well as nonvolatile circuits enabling normally-off instantly-on computing systems [6]. One of the most explored options for beyond CMOS devices is spintronic (nanomagnetic) logic [7–9].

The first commercial spintronic device, magnetic random access memory (RAM) [10], operated by switching magnetization via the Oersted magnetic field of a current. More efficient switching by spin transfer torque (STT) [11,12] gave rise to a new generation of STT-RAM [13] which operates at a smaller required switching current. More recently, the spin Hall effect (SHE) was applied to switching the magnetization [14] of a ferromagnetic (FM) layer in a magnetic tunnel junction (MTJ) device, and the effect is hoped to switch magnetization at an even smaller current with further materials development. Therefore, understanding the spin properties of these materials and their SHE parameters is necessary for estimating the performance of devices and circuits comprising them.

SHE has been observed in elemental metals with a high atomic number: Pt [15], W [16], and Ta [14], and more recently in a topological insulator Bi₂Se₃ [17]. The effect originates from spin-orbit coupling in these materials and is manifested as the creation of spin polarized electrons at the surface of the material [18] when a charge current is applied to the material. If the SHE material is in contact with a ferromagnet (FM), the spin polarized current of the SHE material will be injected into the FM and will be capable of switching its magnetization direction by spin transfer torque. The efficiency of the conversion of the charge current in the SHE material to the spin current injected into the FM is quantified by the spin Hall coefficient θ_{SHE} , which is defined as the ratio of the spin current density and the charge current density, $\theta_{SHE} = J_s/J_c$.

For tantalum, five different published values of the SHE coefficient [14,19–22] have been reported that span a range

of more than an order of magnitude. With such a wide range of values, there is much debate as to the mechanism(s) that produce the spin Hall effect in tantalum, as well as what other mechanisms may be present that produce spin current.

Direct measurement of both the longitudinal and transverse effective fields produced by tantalum that correspond to the in-plane and out-of-plane spin torques were measured reported by several groups [22–25]. In all cases, a significant out-of-plane torque was seen. While the in-plane or Slonczewski torque is known to originate from the SHE, the out-of-plane or fieldlike torque was attributed by Refs. [22,23] to the Rashba effect, although Ref. [22] points out that this model is too simplistic to completely explain their measurement.

In this paper we measure both the in-plane and out-of-plane spin torques produced by tantalum on a FM at various tantalum thicknesses using a ferromagnetic resonance technique. We start by describing a model for the dynamics of the FM's magnetization used to explain the experimental results, the procedure for fabrication of samples, the experimental method, and the results of the measurement. We close with a discussion and interpretation of the experimental results by the coexistence of both the SHE and a constant Rashba-effect spin current originating from the Ta/FM interface.

II. MODEL OF SPIN-ORBIT EFFECTS

To describe the experimental results presented in this paper, we solve the Landau-Lifshitz-Gilbert (LLG) equation for the magnetization of a FM in an oscillating magnetic field that is in contact with a normal metal (NM) exhibiting the SHE. We include in our derivation the often neglected out-of-plane torque term. The full LLG is

$$\frac{d\hat{\mathbf{m}}}{dt} = -\gamma\hat{\mathbf{m}} \times \mathbf{H}_{\text{eff}} + \alpha\hat{\mathbf{m}} \times \frac{d\hat{\mathbf{m}}}{dt} + \gamma\beta_{\parallel}\hat{\mathbf{m}} \times [\hat{\mathbf{s}} \times \hat{\mathbf{m}}] + \gamma\beta_{\perp}\hat{\mathbf{s}} \times \hat{\mathbf{m}}, \quad (1)$$

where \mathbf{m} is the unit vector of the FM's magnetization and \mathbf{s} is the unit vector of the polarization of the spin current injected into the FM from the NM. The quantities \mathbf{H}_{eff} , γ ,

and α are the effective magnetic field (sum of the applied field, demagnetization field, and the anisotropy field), the gyromagnetic ratio, and the damping coefficient, respectively. Lastly, the two quantities, β_{\parallel} and β_{\perp} , are the coefficients for the antidamping (in-plane) and fieldlike (out-of-plane) spin torques, respectively, and have units of magnetic field:

$$\beta_{\parallel} \equiv \varepsilon_{\parallel} \frac{\hbar}{2e} \frac{J_s}{M_s t_m}, \quad \beta_{\perp} \equiv \varepsilon_{\perp} \frac{\hbar}{2e} \frac{J_s}{M_s t_m}. \quad (2)$$

The coefficients ε_{\parallel} and ε_{\perp} are introduced to take into account the efficiency of the spin transfer process [26]. Spin current densities J_s are in units of A/m^2 .

In the presence of an applied magnetic field, the direction of the magnetization of a FM will precess around the direction of the applied magnetic field, at an angle of precession ϕ_p . This typically small change in the direction of magnetization $\Delta \mathbf{m}$ can be calculated from Eq. (1). Since the angle of precession is small, it can be approximated as $|\Delta \mathbf{m}|$, which from Eq. (1) is

$$\phi_p \approx |\Delta \mathbf{m}| = \frac{1}{\Delta(2H_0 + M_s)} \left[(h_y^{\text{rf}} + \beta_{\perp} s_y) B_0 L_A(H) + \left(\beta_{\parallel} \frac{\omega}{\gamma} s_y \right) L_S(H) \right], \quad (3)$$

where Δ is the linewidth of ferromagnetic resonance (FMR), h_y^{rf} is the y component of the rf magnetic field, s_y is the y component of the spin polarization unit vector, and H_0 is the applied field at resonance. The functions L_S and L_A are the symmetric and antisymmetric Lorentzians, respectively:

$$L_A(H) = \frac{\Delta(H - H_0)}{(H - H_0)^2 + \Delta^2}, \quad L_S(H) = \frac{\Delta^2}{(H - H_0)^2 + \Delta^2}. \quad (4)$$

We have assumed here that, due to the large in-plane anisotropy of the thin FM, the precession is primarily in the film plane and the precession of the magnetization is elliptical.

III. MEASUREMENT AND RESULTS

The measured samples were composed of $20 \times 100 \mu\text{m}$ Ta/CoFeB bilayer lines patterned as the center conductor of a coplanar waveguide with Au ground lines and probe pads. The waveguide was patterned on 100 nm of SiN on a silicon wafer substrate. The bilayers were grown by Ar sputtering of Ta and $\text{Co}_{20}\text{Fe}_{60}\text{B}_{20}$ (CoFeB) targets onto a patterned resist followed by a resist lift-off process. Ta was always deposited on top of CoFeB without an airbreak. The thicknesses of the Ta layer ranged between 1 and 8 nm, while the thickness of the CoFeB layer was kept constant at 4 nm. Additionally, a sample with a single 6 nm CoFeB layer was produced for comparison.

Thicknesses were determined by a combination of transmission electron microscopy (TEM) images and resistivity measurements. We estimated an uncertainty in the thicknesses of ± 0.2 nm which was used to estimate errors in all the calculated quantities. Upon exposure to air, oxidation of the top Ta layer resulted in an oxide layer of approximately 3 nm. Resistivities of 1850 and 1400 Ωnm for Ta and CoFeB, respectively, were measured by sheet resistance

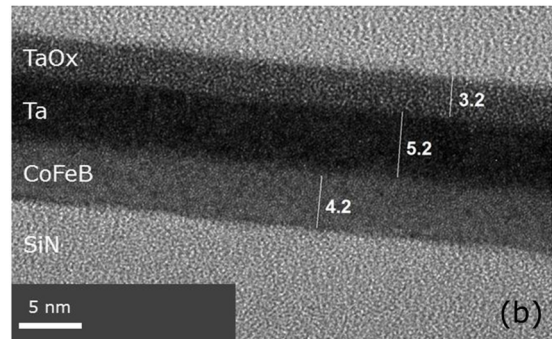
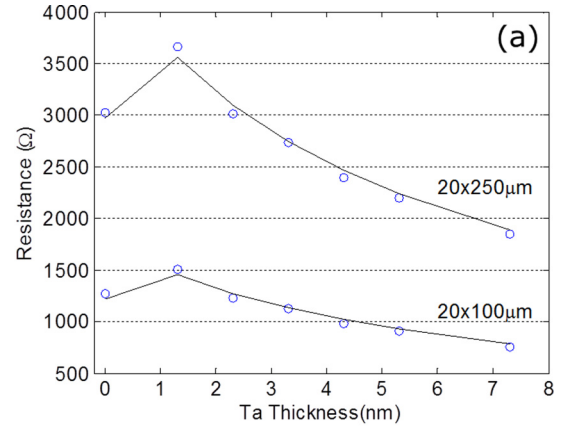


FIG. 1. (Color online) (a) The dc resistance of the Ta/CoFeB lines with 4 nm of CoFeB. Data for both 100 and 250 μm length lines are shown. The circles represent measured data, while the solid lines are calculated from the film resistivities and thicknesses. The data at zero Ta thickness are for a 6 nm CoFeB layer without Ta. (b) TEM cross section image of a $20 \times 100 \mu\text{m}$ bilayer line.

measurements on blanket films. These values were used to calculate the resistances of the bilayer lines and matched well with dc resistance measurements when a contact resistance of approximately 50 Ω is assumed [Fig. 1(a)].

The large and constant resistivity found for all Ta thicknesses indicates that the films are entirely β -phase Ta, which is in line with our experience with Ta films less than 10 nm in thickness. An in-plane magnetoresistance value of $2.1 \times 10^{-3} \pm 0.1 \times 10^{-3}$ for the CoFeB layer was measured for all samples using dc resistance measurements. The possibly different out-of-plane magnetoresistance [27] was not considered due to the large in-plane anisotropy of the CoFeB layer. Further, all applied fields were in plane and less than 0.12 T, much less than the out-of-plane demagnetization field of approximately 1.9 T. (See the M_s values reported below.)

To measure the SHE of Ta, we use the FMR measurement technique developed by Liu *et al.* [15]. In their technique, an rf charge current is sent through a FM/NM bilayer at GHz frequencies. This arrangement of layers and driving frequency has the advantage of emulating that of proposed SHE driven spintronic devices (e.g., the top two layers of an MTJ driven at GHz frequencies).

When this current is injected into a bilayer line, the portion of the current that flows through the NM layer simultaneously creates an in-plane rf magnetic field (the Oersted field) in the

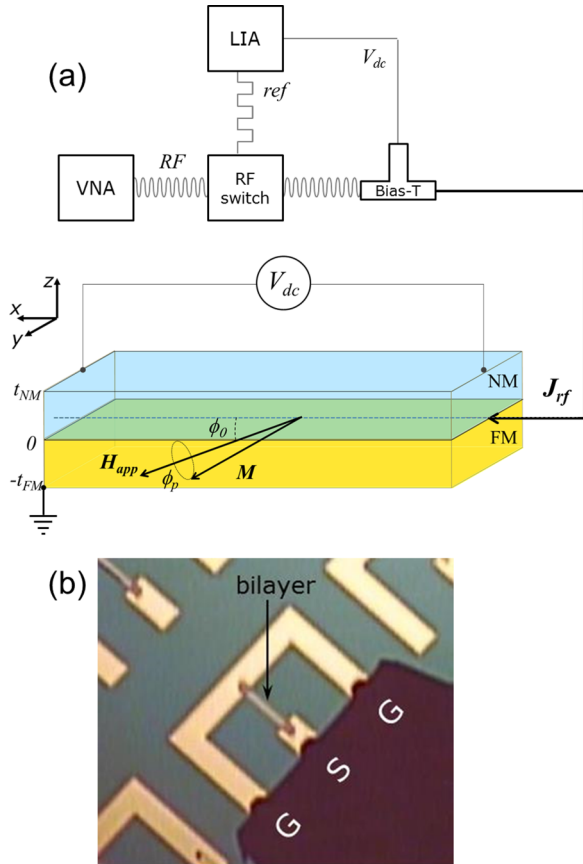


FIG. 2. (Color online) (a) Schematic of the FMR measurement. A vector network analyzer is used as an rf current source. The rf current is modulated by an rf switch and applied to a bilayer of β -Ta on CoFeB. An in-plane magnetic field is also applied to the bilayer at 45° to the direction of the charge current. A dc voltage results and is measured by a lock-in amplifier referenced to the frequency of the rf switch. (b) Image of the rf probe in contact with a coplanar waveguide test structure with a bilayer line as the center conductor.

FM, as well as injecting a spin current into the FM due to the SHE. Both of these effects influence the precession of the magnetization around the direction of the applied field. The oscillation of the angle of magnetization from precession causes an oscillation of the resistance of the FM due to anisotropic magnetoresistance (AMR). Since the frequency of the oscillation is the same as that of the applied rf current, frequency mixing produces a dc voltage that is proportional to both the current flow in the FM and its magnetoresistance.

A schematic of our measurement setup is given in Fig. 2, where a vector network analyzer is shown to force a microwave frequency current into a Ta/CoFeB bilayer. The resulting dc voltage across the length of the line is on the order of microvolts or less, so a lock-in amplifier is used in conjunction with an rf switch that chops the rf current at 1.37 kHz.

The samples' lines form the center conductor of a coplanar waveguide, with the ground lines and probe pads made of Au. Electrical contact is made with $150 \mu\text{m}$ pitch ground-signal-ground (GSG) probes. Measurements were made at frequencies of 7, 8, 9, and 10 GHz with 17 ± 0.5 dBm of rf power at the probe tips. The generated dc voltage was measured

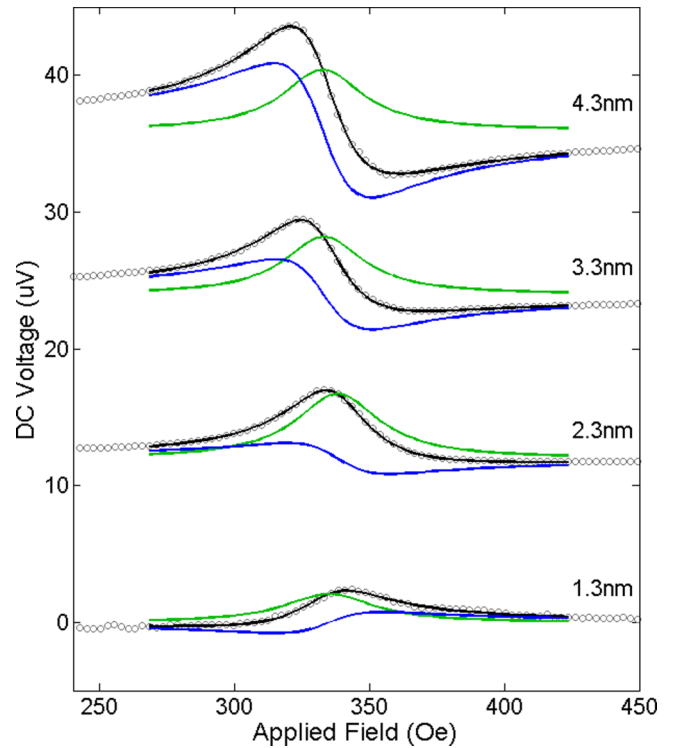


FIG. 3. (Color online) The FMR voltage measured for Ta on 4 nm CoFeB. The labels refer to the Ta thickness. Shown are the measured data (black circles) and fit (black line) to the data using Eq. (5), and the symmetric (green line) and antisymmetric (blue line) components resulting from the fit.

as a function of an applied in-plane magnetic field aligned 45° to the direction of the rf current. All measurements were made at room temperature.

Using the expression for the precession angle of the magnetization in Eq. (3), the dc voltage as a function of applied field strength can be shown to equal

$$\begin{aligned}
 V_{\text{dc}} &= -\frac{1}{2} I_{\text{rf}} \Delta R_{\text{AMR}} \frac{\sin(2\phi_0) \cos \phi_0}{\Delta (2H_0 + M_s)} \frac{\omega}{\gamma} \\
 &\times \left[\sqrt{\frac{B_0}{H_0}} (h_{\text{rf}} + \beta_{\perp}) L_A(H) + \beta_{\parallel} L_S(H) \right] \\
 &\equiv V_A L_A(H) + V_S L_S(H). \quad (5)
 \end{aligned}$$

From Ampere's law, the Oersted field in the FM created by the NM is $h_{\text{rf}} = J_c^{\text{NM}} t_{\text{NM}}/2$.

In Fig. 3, the measured dc voltage as a function of applied field strength is shown for four different Ta thicknesses at a driving frequency of 7 GHz. The measured voltage versus applied field is fitted to the sum of a symmetric and an antisymmetric Lorentzian, in accordance with Eq. (5). The parameters of the fit are the weights of the Lorentzians, V_A and V_S , and the resonant applied field and linewidth, H_0 and Δ . There was also a voltage offset present in the data in addition to the symmetric and antisymmetric Lorentzians that is not encompassed in Eq. (5). We provide no explanation for this offset but have found it to vary as the $\sin(\phi_0)$ and changes sign with a change in sign of the magnetization. We have included

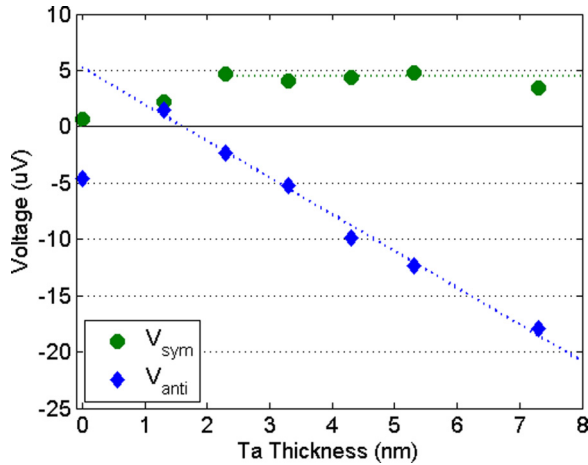


FIG. 4. (Color online) Voltage of the symmetric (green circles) and antisymmetric (blue diamonds) components vs Ta thickness on 4 nm CoFeB at 7 GHz. The data points at zero Ta thickness are for a single 6 nm layer of CoFeB. The slope and intercept is a linear fit to V_{anti} (dashed blue line) and the value of V_{sym} at the higher Ta thickness (dashed green line) is also shown. Voltage error bars are hidden by the markers, but are always less than $0.28 \mu\text{V}$.

an offset into our curve fit, although its value is not used for any calculations.

Data for the symmetric and antisymmetric components of the dc voltage versus Ta thickness, V_S and V_A , respectively, at a 7 GHz driving frequency are plotted in Fig. 4. The statistical error (2σ) for all values of V_S and V_A measured at the four frequencies was always less than $0.28 \mu\text{V}$.

The fit values for the resonant field H_0 versus the driving frequency can be fit to the Kittel equation for thin films, $\omega^2 = \gamma\sqrt{H_0(H_0 + M_s)}$, to determine the saturation magnetization M_s of the CoFeB layer. The value of M_s for the CoFeB only sample, $1.92 \pm 0.01 \text{ T}$, was found to be larger than that of the samples deposited with Ta, $1.84 \pm 0.01 \text{ T}$, averaged over six samples (Fig. 5). For comparison, we measured the 5.3 nm Ta sample on a superconducting quantum interference device (SQUID) magnetometer and obtained a value of $1.86 \pm 0.05 \text{ T}$

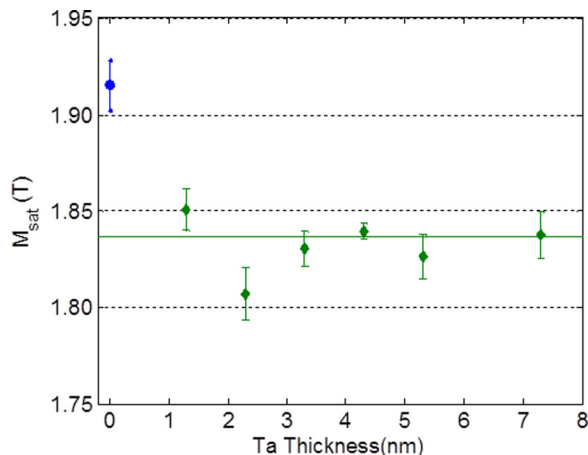


FIG. 5. (Color online) The saturation magnetization M_{sat} determined for each sample from a fit to the Kittel equation.

for M_s , which is in agreement with the values from the FMR measurement.

In regards to the difference in M_s for the CoFeB only sample, it is known that Ta sputtered onto CoFeB can create a magnetic dead layer [28]. The dead layer itself will not change the magnetization (i.e., the magnetic moment per unit volume is unchanged), so we ascribe the reduction in M_s to an intermediate layer at the interface in which the magnetization CoFeB is reduced but not eliminated. We have not characterized the thickness of the magnetic dead layer, so for our calculations of θ_{SH} below, we have used the thickness determined as described in this section. This, in general, will cause our value for θ_{SH} to be larger by an undetermined amount.

The SHE coefficient can be calculated from the symmetric (V_S) and antisymmetric (V_A) components of the measured dc voltage versus Ta thickness. Assuming a perfectly spin conducting interface, defined by an infinitely large interface spin-mixing conductance G_{mix} [29], the data for V_S is expected to follow the relation $V_S(t_{\text{NM}}) = V_S^\infty [1 - \text{sech}(\frac{t_{\text{NM}}}{\lambda_{\text{sf}}})]$, with V_S^∞ being the large thickness limit of V_S . This value is indicated by the dashed green line in Fig. 4. The dependence of V_A on Ta thickness is linear, but has a positive offset. The offset results in V_A becoming zero and changing sign at a Ta thickness of 1.7 nm. This also clearly seen in Fig. 3, where the antisymmetric component of the fit to data is seen to change sign between the 1.3 and 2.3 nm sample. The effect was also observed by Ref. [24] for a CoFeB/Ta bilayer, although a systematic study of the thickness dependences was not shown.

We ascribe the positive offset in V_A with thickness to a fieldlike spin torque originating from an interface spin-orbit coupling effect (also referred to as the Rashba effect), which we explain later in this paper. Since this is an interface effect, we assume that the fieldlike torque is independent of Ta thickness.

The spin Hall coefficient θ_{SH} can be calculated from V_S^∞ and the slope of V_A versus Ta thickness V_A^{slope} from the equation

$$\theta_{\text{SH}} = \left(\frac{V_S^\infty}{V_A^{\text{slope}}} \right) \sqrt{1 + \frac{M_s}{H_0} \frac{e}{\hbar} \mu_0 M_s t_{\text{FM}}}, \quad (7)$$

where we have made the assumption that β_\perp is independent of thickness.

For the data shown in Fig. 4, and data taken at frequencies of 8, 9, and 10 GHz, we calculate a spin Hall coefficient for β -Ta of -0.11 ± 0.01 . Our value is lower than that of 0.15 ± 0.03 reported by Ref. [14] for the same measurement technique. This is due to the fact that, in Ref. [14], the value was based on only a single Ta thickness, and hence no accounting of the offset in V_A versus Ta thickness could be included. Using their expression for and using the value for V_A only, we calculate for a similar thickness of Ta and CoFeB, CoFeB(4)/Ta(7.3), a value of -0.13 ± 0.03 , indicating that both measurements are in agreement, if not in interpretation. Our value for θ_{SH} is in good agreement with the two other values reported in Ref. [14], both of which are -0.12 ± 0.03 , obtained from the dependence of damping on a dc bias current, and the critical current to switch a magnetic tunnel junction device.

Comparing to other published data, our value for θ_{SHE} is in very good agreement with that reported by Ref. [22] of -0.11 (no errors reported), but is considerably less than the

value of -0.19 (no errors reported) reported by Ref. [20]. The discrepancy seems too large to be explained by sample variation. One possibility is that, in Ref. [20], it was assumed that only the SHE, an in-plane torque, was present to assist in switching a perpendicularly magnetized magnet. Not including the out-of-plane spin torque would make the in-plane torque produced by SHE to appear larger than it actually is.

Our value for θ_{SHE} is also an order of magnitude larger than the values of $-0.02(+0.008, -0.015)$ reported by Ref. [21] and 0.0037 ± 0.0011 reported by Ref. [19]. It should be noted that the value reported in Ref. [21] is for a Ta/yttrium iron garnet (YIG) bilayer, and that reported in Ref. [19] is for a Ta to Cu spin channel to a permalloy system. It is reasonable to expect that the spin current transferred across a NM/FM interface is dependent on the materials at the interface, and could thus explain the differences in reported values. This would indicate that the spin Hall coefficient is not an intrinsic property of Ta (or other NM) but includes the efficiency of spin transmission across the NM/FM interface.

We can also determine the ratio of the two spin torque terms, β_{\perp} and β_{\parallel} , from the thickness where V_A goes to zero, $t_{\text{NM}} = 1.7$ nm. At this thickness, the torque from the Oersted field of the charge current is canceled by the out-of-plane spin torque. From (2), the ratio of the effective spin torque fields is

$$\frac{\beta_{\perp}}{\beta_{\parallel}} = -\frac{e\mu_0 M_s t_{\text{FM}} t_{\text{NM}}}{\hbar\theta_{\text{SH}}}, \quad (8)$$

which yields a value of 0.16 ± 0.03 .

Comparison to other reported values of this ratio for Ta is problematic as published data are reported on various FM layers, anisotropy directions, and different layer thicknesses, all of which may confound comparisons of the reported ratios. For example, Ref. [22] reported a value of 3.7 for Ta(2)/CoFeB(0.8)/MgO(2), which is clearly much larger than ours, but with a much thinner CoFeB layer with perpendicular anisotropy. In Ref. [23], a CoFeB FM with perpendicular anisotropy was also used with a reported ratio of 3.3 for Ta(1.3)/CoFeB(1)/MgO(2). However, they did discover that this ratio decreased with increasing CoFeB thickness, equaling one at a thickness of approximately 1.5 nm. Our value of 4 nm for CoFeB is at least consistent with this observation.

In Ref. [24], a value of 0.38 is reported for Ni₈₀Fe₂₀(2)/Ta(5). While the FM is not the same, the value is at least of the same order of magnitude as ours. Interestingly, Ref. [24] also reported a value of 0.41 for a Pt(5) layer, which is essentially the same as that for the Ta layer, even though the two metals are known to have different values for θ_{SH} , which is equal to $+0.07$ for Pt [15]. This may indicate a link between the sources of the in-plane and out-of-plane spin torques.

IV. EXPLANATION OF THE THICKNESS DEPENDENCE OF THE SPIN TORQUE

As shown in Eq. (5), the symmetric and antisymmetric components of the measured dc voltage originate from antidamping and fieldlike spin torques, respectively. We attribute the thickness dependence of the spin torques as arising from spin currents produced by both the SHE of the bulk β -Ta and the Rashba effect at the Ta/CoFeB interface. In particular, we

identify the Rashba effect as the source of the positive offset of the antisymmetric component seen in Fig. 4.

A similar offset in the thickness dependence of the inverse SHE current from spin pumping measurements was observed by Hou *et al.* [30] in bismuth/permalloy bilayers. They were able to explain the offset as originating from a distinct interface layer with a spin Hall coefficient and spin diffusion length different from that of the bulk material. However, in the case of Ta/CoFeB bilayers measured in this study, we can explain the origin of the offset to the spin current produced at the interface by the Rashba effect.

We use the semiclassical drift-diffusion model developed by Ref. [31] to model the presence of an interface spin-orbit coupling (ISOC) effect (referred to as the Rashba effect) and a bulk spin-orbit coupling effect (BSOC) (referred to as the spin Hall effect). The semiclassical model comprehends (a) BSOC and ISOC, (b) the effect of finite (G_{mix}) spin-mixing conductance between the FM and NM, (c) the effect of the relative ratio of imaginary [$\text{Im}(G_{\text{mix}})$] and real [$\text{Re}(G_{\text{mix}})$] components of the spin-mixing conductance, (d) the thickness effects due to scaling of the spin-mixing conductance which depends on the available states in the NM, $\tilde{G}_{\text{mix}}(t) = 2G_{\text{mix}}\rho_{\text{FM}}\lambda_{\text{sf}}\tanh(t/\lambda_{\text{sf}})$, and (e) the thickness effects due to the spin diffusion in the NM.

We write the interfacial torque on the FM (assuming spin current absorption at the interface as $l_{\text{sf-FM}}$ approaches zero) [31],

$$T = \delta(z)\frac{g\mu_B j_0}{2e}[\tau_d \hat{M} \times (\hat{M} \times \hat{y}) + \tau_f \hat{M} \times \hat{y}], \quad (9)$$

where \hat{y} is the direction of the spin moment of the injected electrons propagating along \hat{z} , the interface vector for the FM to NM interface (Fig. 6).

We note that the ISOC as well as BSOC can generate damping and fieldlike torques. BSOC generates predominately a(n) (anti)damping torque. However, BSOC can also generate a fieldlike torque component proportional to the imaginary part of the spin-mixing conductance of the NM to FM interface. ISOC generates a predominantly fieldlike torque, but can also generate a damping torque depending on the exact dephasing mechanism inside the FM [31]. However, it has been noted that while both ISOC and BSOC contribute to both τ_d and τ_f only, BSOC exhibits a strong dependence on the thickness of the NM.

We include both the ISOC and BSOC contributions to the damping and fieldlike contributions to the spin torques to explain the torque dependence in a FM/NM bilayer. The damping torque in the presence of ISOC and BSOC can be written as

$$\begin{aligned} \tau_d = \tau_{\text{dBSOC}} + \tau_{\text{dISOC}} = \theta_{\text{SHE}} \frac{(1 - e^{-t/\lambda_{\text{sf}}})^2}{(1 + e^{-2t/\lambda_{\text{sf}}})} \\ \times \left[\frac{|\tilde{G}^{\uparrow\downarrow}|^2 + \text{Re}[\tilde{G}^{\uparrow\downarrow}]\tanh^2(t/\lambda_{\text{sf}})}{|\tilde{G}^{\uparrow\downarrow}|^2 + 2\text{Re}[\tilde{G}^{\uparrow\downarrow}]\tanh^2(t/\lambda_{\text{sf}}) + \tanh^4(t/\lambda_{\text{sf}})} \right] \\ + \tau_{\text{dISOC}}, \end{aligned} \quad (10)$$

where we included a NM thickness independent contribution to the damping spin torque arising from ISOC. $\tilde{G}_{\text{mix}}(t)$ is a scaled spin-mixing conductance accounting for thickness

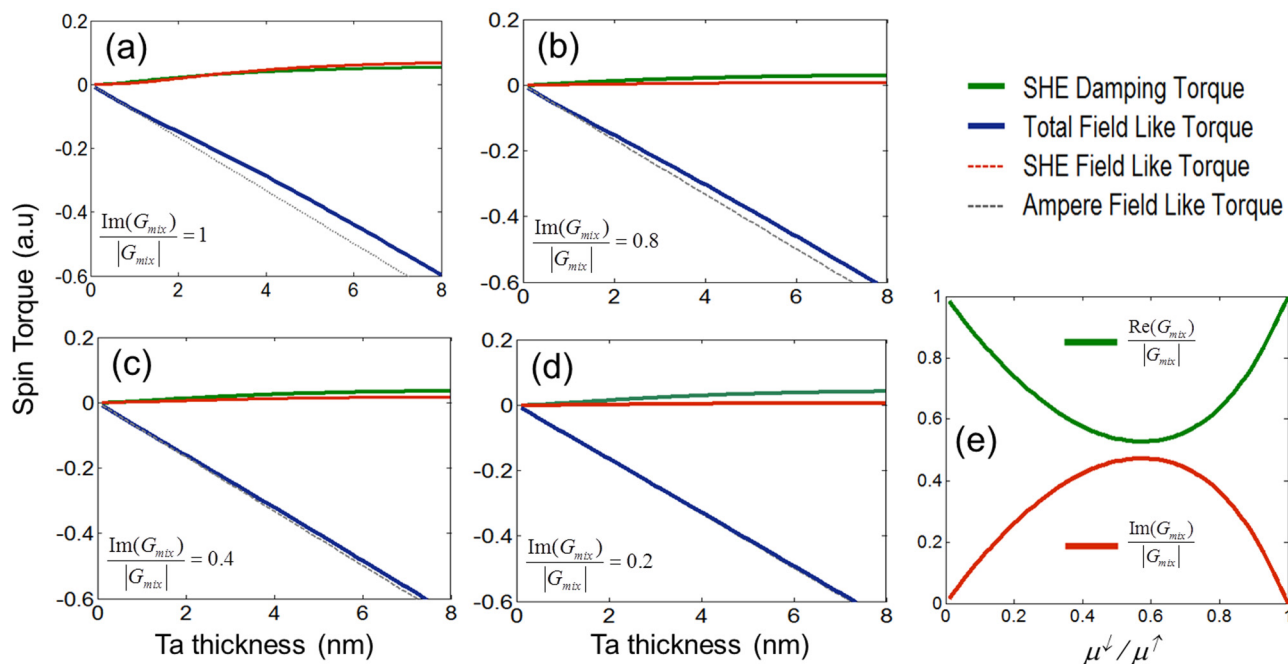


FIG. 6. (Color online) The BSOC (SHE) only scenario. Plotted are the calculated spin torque vs thickness dependences if SHE and the ampere field were the only spin/magnetic torques present in the system for (a) the ratio of the imaginary part of the spin-mixing conductance $R = 1$, (b) $R = 0.8$, (c) $R = 0.4$, (d) $R = 0.2$. The fieldlike torque produced by SHE due to the presence of spin reflection at the NM/FM interface cannot produce a sign change in the fieldlike torque combined with a positive constant offset. The fieldlike torque from SHE approaches zero for zero thickness. (e) Effect of varying interface potentials on the ratio of the imaginary part of the spin-mixing conductance.

induced effects. The fieldlike torque in the presence of ISOC and BSOC can be written as

$$\begin{aligned} \tau_f &= \tau_{\text{fBSOC}} + \tau_{\text{fISOC}} + \tau_{\text{fAmpere}} \\ &= \theta_{\text{SHE}} \frac{(1 - e^{-t/\lambda_{\text{sf}}})^2}{(1 + e^{-2t/\lambda_{\text{sf}}})} \\ &\quad \times \left[\frac{\text{Im}[\tilde{G}^{\uparrow\downarrow}] \tanh^2(t/\lambda_{\text{sf}})}{|\tilde{G}^{\uparrow\downarrow}|^2 + 2\text{Re}[\tilde{G}^{\uparrow\downarrow}] \tanh^2(t/\lambda_{\text{sf}}) + \tanh^4(t/\lambda_{\text{sf}})} \right] \\ &\quad + \tau_{\text{fISOC}} + \frac{CV}{\rho(L/w)} t, \end{aligned} \quad (11)$$

where the third term is the ampere field due to the current. A fixed thickness independent contribution is added due to the fieldlike contribution from the interface spin-orbit effect.

To deconvolve what could be happening, we first consider the possibility of a BSOC as the only explanation for the measured damping and fieldlike torques as a function of the NM thickness. We vary the reflectivity ratio R from 1 to 0.2, where R is defined as the ratio

$$R \equiv \frac{\text{Im}(G_{\text{mix}})}{|G_{\text{mix}}|}. \quad (12)$$

Figure 6 shows the expected dependence of BSOC assuming the presence of just a BSOC and no ISOC. The damping torque (τ_{dBSOC}) from BSOC saturates to a maximum value at a thickness $t > \lambda_{\text{sf}}$. The fieldlike torque from BSOC (τ_{fBSOC}) exhibits a similar saturation near $t > \lambda_{\text{sf}}$. In an experimental measurement using the FMR technique this would result in a constant offset only at $t > \lambda_{\text{sf}}$, as shown in Figs. 6(a)–6(d). Figure 6(a) shows the case for $R = 1$, implying that the

spin-mixing conductance is purely imaginary. The damping and fieldlike torque from BSOC are comparable in this case, both approaching the same value at $t > \lambda_{\text{sf}}$. The large fieldlike contribution from BSOC would then lead to a large offset, as shown in Fig. 6(a), only at $t > \lambda_{\text{sf}}$ with a fieldlike torque approaching zero at zero thickness. The contribution to the measured fieldlike torque reduces as R approaches 0. For a metal to metal surface, R is usually a small number [29], but for our explanation below, we will assume that even in the unlikely case that R is not small, our data cannot be explained with spin torques produced by BSOC only or by ISOC only.

We use the following arguments against a BSOC only explanation of the measured data. First, τ_{fBSOC} will result in a thickness varying offset to the total fieldlike torque. Second, the fieldlike torque from BSOC (τ_{fBSOC}) produces a measurable offset in the fieldlike torque as R approaches one. Lastly, we show below that for spherical Fermi surfaces $R < 0.5$, we were unable to produce a large positive intercept [$H_{\text{f-intercept}}(t=0)$] and a sign change for the total fieldlike torque for R between 0.1 and 1. We further note that for a special case where all the Fermi surfaces are spherical and the same size, where the spin dependent transmission is due to a surface potential,

$$\begin{aligned} \text{Re}(G) &= \frac{1}{2} + \frac{u^\uparrow u^\downarrow}{2(u^\uparrow + u^\downarrow)} \left[u^\downarrow \ln \left(\frac{u^\downarrow^2}{1 + u^\downarrow^2} \right) \right. \\ &\quad \left. + u^\uparrow \ln \left(\frac{u^\uparrow^2}{1 + u^\uparrow^2} \right) \right], \end{aligned} \quad (13)$$

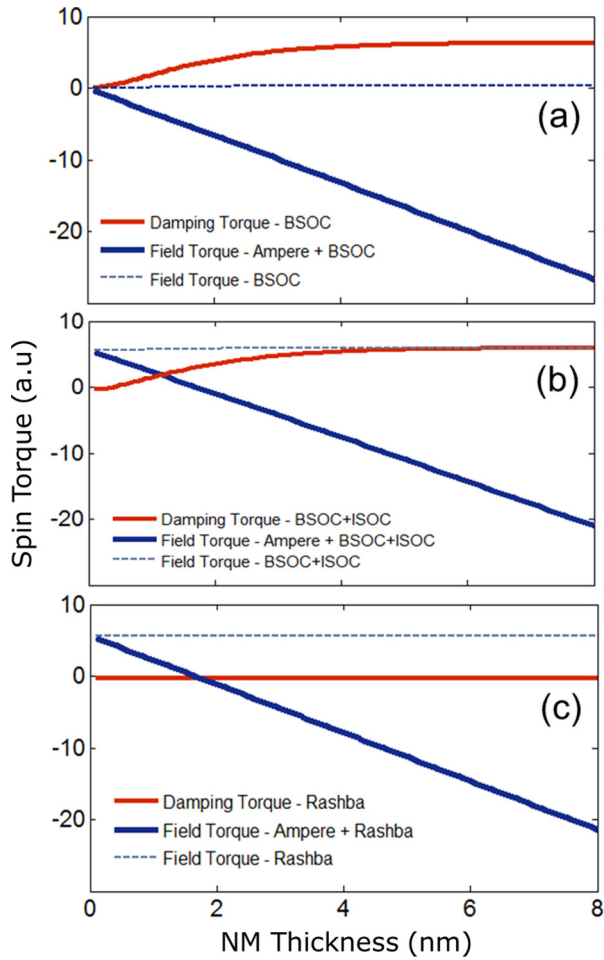


FIG. 7. (Color online) The calculated spin torque vs NM thickness for varying relative strengths of ISOC and BSOE. (a) BSOE only. (b) ISOC and BSOE present in equal strengths. (c) ISOC only.

$$\text{Im}(G) = \frac{u^\uparrow u^\downarrow}{2(u^\uparrow + u^\downarrow)} (u^\downarrow [\pi - 2 \tan^{-1} u^\downarrow] - u^\uparrow [\pi - 2 \tan^{-1} u^\uparrow]), \quad (14)$$

where u^\uparrow, u^\downarrow represent the strength of the spin dependent potential $V = (u^\uparrow \text{ or } \downarrow \hbar^2 k_F / m) \delta(z)$ at the interface [29,31]. The relation between the ratio $R = \text{Im}(G)/|G|$ and u^\uparrow/u^\downarrow is plotted in Fig. 6(e), showing that under the spherical Fermi surface assumption, R is < 0.5 . The typical experimental estimation of R for an FM to NM interface is given in Ref. [29].

The experimentally measured damping and fieldlike torques can be explained using a semiclassical diffusive model that includes the presence of both BSOE and ISOC effects simultaneously. We also show three scenarios for the relative strength of the ISOC and BSOE effects in Figs. 7(a)–7(c). In all the scenarios, the measured fieldlike torque exhibits a linear increase due to increasing current as the resistance of the NM reduces with increasing thickness. The linear increase in the ampere fieldlike torque with thickness is consistent with a constant resistivity as confirmed by two-layer sheet resistance fits (Fig. 1). When BSOE is the only contribution to the spin torque [Fig. 7(a)], the measured fieldlike torque is mostly attributed to the ampere torque. BSOE does generate a small fieldlike torque (blue dotted line) due to the imaginary component of the spin-mixing conductance. We use an $R = 0.1$ to include the effect of a fieldlike torque generated from BSOE. However, this scenario (BSOE only) does not produce an offset in the fieldlike torque. When ISOC is the only contribution to the spin torque, the ISOC damping torque is independent of thickness and has a small constant $-V_e$ value [31]. Therefore, this scenario (ISOC only) does not explain the measured damping torque. When both ISOC and BSOE are included in the model [Fig. 7(b)], the damping torque exhibits a saturating and increasing behavior consistent with measurement. The fieldlike torque in the BSOE+ISOC scenario exhibits a linear increase in magnitude (due to an increasing ampere field with increasing NM thickness) and a constant thickness independent offset corresponding to an ISOC fieldlike contribution.

We fit the experimental data with the diffusive model to extract the relative strength of the ISOC and BSOE spin torques. The parameters used for the fitting are shown in Table I. We estimate an electron mean free path of 0.5 nm based on the electron density of β -Ta ($5.58 \times 10^{22} \text{ cm}^{-3}$) assuming one valence electron per atom. Figure 8(a) shows the fitting of the fieldlike torque with an ampere torque combined with a large positive offset arising from an interface spin-orbit torque. Measurements were repeated at 7, 8, 9, and 10 GHz on all seven samples. A clear sign change in the measured antisymmetric component at 1.3 nm is observed for all four measurement frequencies. A value of 2.5 nm for the spin diffusion length λ_{sf} was also extracted from the fit and is in good agreement with the two previously published values for Ta, 2.7 ± 0.4 nm [19] and 1.8 ± 0.7 nm [21].

The behavior of single-layer CoFe plotted at zero NM thickness exhibits a negative fieldlike torque and a small positive damping torque. A nonzero antisymmetric component in the FMR signal for a single-layer FM has already been reported

TABLE I. The parameters used for fitting to the experimental data to a diffusive model that includes the presence of both BSOE and ISOC.

| Quantity | Value | Expression | Source/Ref. |
|---|--|---|-------------|
| Density (D) | 16.69 g/cm ³ | | |
| Resistivity (ρ_N) | 185 $\mu\Omega$ cm | Measured | |
| Spin-mixing conductance (G_{mix}) | $2.16 \times 10^{14} \Omega^{-1}/\text{m}^2$ | Eq. (11) | [29] |
| Fermi wave vector ($k_{F,\beta\text{-Ta}}$) | 11.8 nm ⁻¹ | $k_F = (3\pi^2 D N_A N_V / Z)^{1/3}$ | [34] |
| Mean free path ($\lambda_{\beta\text{-Ta}}$) | 0.47 nm | $\lambda_n = (h/2e^2)\sigma^3 \pi k_F^{-2}$ | [34] |
| SHE coefficient | -0.11 | Eq. (7) | |
| Spin diffusion length (λ_{sf}) | 2.5 nm | Eq. (11) | |

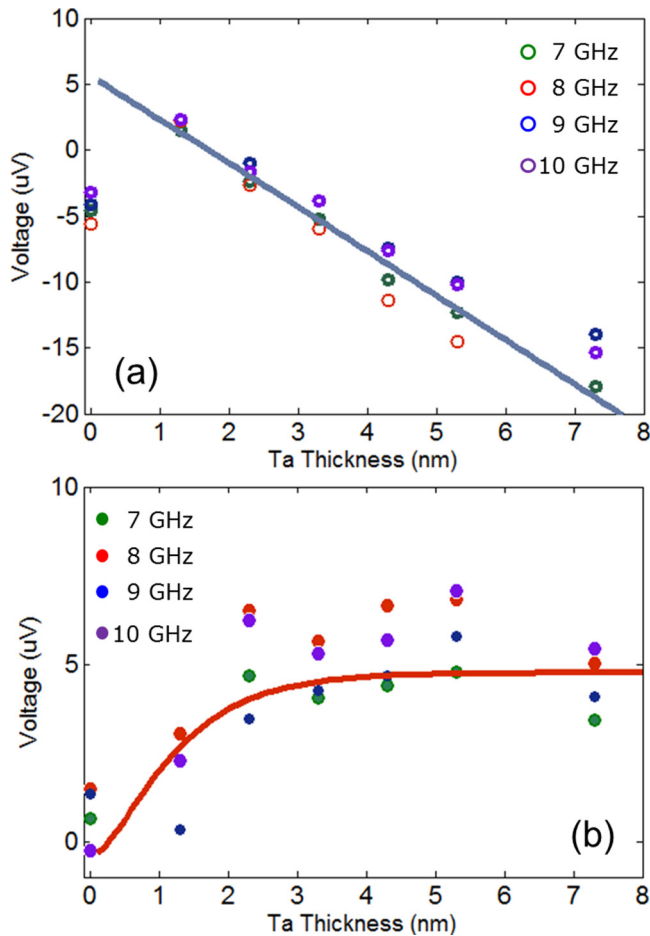


FIG. 8. (Color online) Fit of the ISOC+BSOC to measured data of CoFe/ β -Ta bilayers. The measured (a) fieldlike torques and (b) damping torques are consistent with the coexistence of a strong fieldlike interface spin-orbit torque with a bulk spin-orbit torque. Voltage error bars are hidden by the markers, but are always less than $0.28 \mu\text{V}$.

in a similar experiment and attributed to the nonuniformity of the FM [32] or a potential contribution from local spin-orbit effects in the FM [29]. We also note that the sign of the antisymmetric component observed at zero Ta thickness is

opposite to the sign of the offset attributed to ISOC. We further note that spin pumping from the FM combined with an inverse Rashba-Edelstein effect (IREE) or inverse spin Hall effect (ISHE) can produce a dc mixing voltage. However, IREE and ISHE contribute only to the symmetric part of the FMR measurement [17,33], leading to a correction in the damping torques. Our conclusion regarding the presence of a strong fieldlike ISOC contribution therefore should not be affected by the contribution from IREE or ISHE.

V. CONCLUSIONS

In summary, we have performed FMR measurements of β -Ta deposited on $\text{Co}_{20}\text{Fe}_{60}\text{B}_{20}$ bilayers with β -Ta thicknesses ranging between 1 and 8 nm. From this data we have extracted both the damping and fieldlike torques exerted on the CoFeB layer. The damping torque was found to increase and saturate with increasing Ta thickness, as expected from spin diffusion theory. The fieldlike torque, however, increased linearly (negatively) with Ta thickness, but with a positive offset, opposite to that produced by the Oersted field of the Ta layer. This resulted in the net fieldlike torque becoming zero at approximately 1.5 nm Ta thickness, and becoming positive for smaller thicknesses.

The spin Hall coefficient of β -Ta was calculated to be -0.11 ± 0.01 using the ratio of the saturated value of the symmetric component and the slope of the antisymmetric component versus Ta thickness, the use of the slope of the antisymmetric component being necessary in order to remove the constant positive fieldlike torque. The saturation magnetizations for the CoFeB layers were also calculated from the FMR data, where the value of 1.84 ± 0.01 T for the samples deposited with Ta was found to be smaller than that of a single layer of CoFeB, which had a value of 1.92 ± 0.01 T.

We attribute the thickness dependence of the spin torques as arising from spin currents produced by both the SHE of the bulk β -Ta and the Rashba effect at the Ta/CoFeB interface. In particular, we identify the Rashba effect as the source of the positive thickness independent offset of the antisymmetric component. From fitting measured data to a model that includes both bulk and interface spin-orbit coupling sources for spin currents, we have determined the spin diffusion length for β -Ta to be 2.5 nm.

- [1] International Technology Roadmap for Semiconductors, 2013, <http://www.itrs.net/>.
- [2] K. Bernstein, R. Cavin III, W. Porod, A. Seabaugh, and J. Welsler, *Proc. IEEE* **98**, 2169 (2010).
- [3] D. Nikonov and I. Young, *Proc. Int. Electron Devices Meet.* **25.4.1** (2012).
- [4] D. E. Nikonov and I. A. Young, *Proc. IEEE* **101**, 2498 (2013).
- [5] R. Sarpeshkar, *Ultra Low Power Bioelectronics* (Cambridge University Press, Cambridge, UK, 2010).
- [6] H. Yoda, S. Fujita, N. Shimomura, E. Kitagawa, K. Abe, K. Nomura, H. Noguchi, and J. Ito, *Proc. Int. Electron Devices Meet.* **11.3.1** (2012).
- [7] D. E. Nikonov and G. I. Bourianoff, *J. Supercond. Novel Magn.* **21**, 479 (2008).
- [8] Y. Zhang, W. Zhao, J.-O. Klein, W. Kang, D. Querlioz, Y. Zhang, D. Ravelosona, and C. Chappert, in *Design, Automation and Test in Europe Conference and Exhibition (DATE), 2014* (IEEE, New York, 2014), pp. 1–6.
- [9] W. Kang, W. Zhao, Z. Wang, J.-O. Klein, Y. Zhang, D. Chabi, Y. Zhang, D. Ravelosona, and C. Chappert, in *Proceedings of the 19th Asia and South Pacific Design Automation Conference (ASP-DAC)* (IEEE, New York, 2014), pp. 676–683.
- [10] W. J. Gallagher and S. S. P. Parkin, *IBM J. Res. Dev.* **50**, 5 (2006).
- [11] M. Tsoi, A. G. M. Jansen, J. Bass, W.-C. Chiang, M. Seck, V. Tsoi, and P. Wyder, *Phys. Rev. Lett.* **80**, 4281 (1998).
- [12] J. A. Katine, F. J. Albert, R. A. Buhrman, E. B. Myers, and D. C. Ralph, *Phys. Rev. Lett.* **84**, 3149 (2000).

- [13] M. Hosomi *et al.*, *Proc. Int. Electron Devices Meet. Tech. Dig.* **459** (2005).
- [14] L. Liu, C.-F. Pai, Y. Li, H. W. Tseng, D. C. Ralph, and R. A. Buhrman, *Science* **336**, 555 (2012).
- [15] L. Liu, T. Moriyama, D. C. Ralph, and R. A. Buhrman, *Phys. Rev. Lett.* **106**, 036601 (2011).
- [16] C.-F. Pai, L. Liu, Y. Li, H. W. Tseng, D. C. Ralph, and R. A. Buhrman, *Appl. Phys. Lett.* **101**, 122404 (2012).
- [17] A. R. Mellnik *et al.*, *Nature (London)* **511**, 449 (2014).
- [18] *Spin Physics in Semiconductors*, edited by M. I. Dyakonov (Springer, Berlin, 2008), Vol. 157.
- [19] M. Morota, Y. Niimi, K. Ohnishi, D. H. Wei, T. Tanaka, H. Kontani, T. Kimura, and Y. Otani, *Phys. Rev. B* **83**, 174405 (2011).
- [20] D. Bhowmik, L. You, and S. Salahuddin, *Proc. Int. Electron Devices Meet.* **29.7.1** (2012).
- [21] C. Hahn, G. de Loubens, O. Klein, M. Viret, V. V. Naletov, and J. Ben Youssef, *Phys. Rev. B* **87**, 174417 (2013).
- [22] X. Qiu, P. Deorani, K. Narayanapillai, K.-S. Lee, K.-J. Lee, H.-W. Lee, and H. Yang, *Sci. Rep.* **4**, 4491 (2014).
- [23] J. Kim, J. Sinha, M. Hayashi, M. Yamanouchi, S. Fukami, T. Suzuki, S. Mitani, and H. Ohno, *Nat. Mater.* **12**, 240 (2013).
- [24] X. Fan, J. Wu, Y. Chen, M. J. Jerry, H. Zhang, and J. Q. Xiao, *Nat. Commun.* **4**, 1799 (2013).
- [25] J. Torrejon, J. Kim, J. Sinha, S. Mitani, M. Hayashi, M. Yamanouchi, and H. Ohno, *Nat. Commun.* **5**, 4655 (2014).
- [26] A. A. Kovalev, G. E. W. Bauer, and A. Brataas, *Phys. Rev. B* **75**, 014430 (2007).
- [27] A. Kobs, S. Heße, W. Kreuzpaintner, G. Winkler, D. Lott, P. Weinberger, A. Schreyer, and H. P. Oepen, *Phys. Rev. Lett.* **106**, 217207 (2011).
- [28] K. Oguz, P. Jivrajka, M. Venkatesan, G. Feng, and J. M. D. Coey, *J. Appl. Phys.* **103**, 07B526 (2008).
- [29] A. Brataas, G. E. W. Bauer, and P. J. Kelly, *Phys. Rep.* **427**, 157 (2006).
- [30] D. Hou *et al.*, *Appl. Phys. Lett.* **101**, 042403 (2012).
- [31] P. M. Haney, H.-W. Lee, K.-J. Lee, A. Manchon, and M. D. Stiles, *Phys. Rev. B* **87**, 174411 (2013).
- [32] A. Tsukahara, Y. Ando, Y. Kitamura, H. Emoto, E. Shikoh, M. P. Delmo, T. Shinjo, and M. Shiraiishi, *Phys. Rev. B* **89**, 235317 (2014).
- [33] Y. Tserkovnyak, A. Brataas, and G. E. W. Bauer, *Phys. Rev. B* **66**, 224403 (2002).
- [34] C. Kittel, *Introduction to Solid State Physics*, 8th ed. (John Wiley & Sons, Inc., New Jersey, 2005), p. 140.